

# CONSIDERATION OF TWO DIMENSIONAL SURFACE ROUGHNESSES IN QUANTITATIVE XPS ANALYSIS

GY. VARSÁNYI, GY. MINK\*, K. RÉE and M. MOHAI\*

Department of Physical Chemistry,  
Technical University, H-1521 Budapest

Received April 15, 1986

## Abstract

The effect of two dimensional surface roughnesses on the intensities of XPS peaks have been investigated. The following models have been studied: square base pits with side walls perpendicular to the surface in chequered position, square base pyramid shaped pits touching each other by their edges, square base pyramids touching each other by their bottom edges, and spheres in closest packing with a planar tangent surface. On the latter model also the effect of ion etching has been studied. The application of the results are demonstrated on two quantitative surface analytical problems.

## Introduction

When analyzing quantitatively layer structures of surfaces one obtains results often very far from reality if the evaluation of the intensity ratios of the XPS peaks is based on formulae valid only for planar surfaces. Fadley and cow. [1] elaborated a method considering the effect of surface roughnesses on peak intensities by very detailed calculations. They took into account only one dimensional surface figures. Later, Wagner and Brünner [2] compared the intensity dependence of photoemission peaks of electrons coming from bulk phase or surface layer on their exit angle calculated with one dimensional surface figures, to those of electrons coming out from planar layers of equal thicknesses. As the surface is, however, two dimensional, the roughnesses have to be imagined in two dimensions when the results are somewhat different from those of calculations based on the supposition of one dimensional forms [1].

If the bulk material is denoted by an index  $t$  while the layer forming materials by running numbers, the peak intensity of the bulk material is given by

$$I_t = I_{t0} \prod_{i=1}^n \exp [-d_i / (\lambda_{ti} \cos \vartheta)] \quad (1)$$

supposing that the bulk phase is covered by  $n$  different layers, the thickness of one layer is  $d_i$ ,  $\lambda_{ii}$  stands for the escape depth of the electron emitted by the bulk material in the  $i$ -th layer while  $\vartheta$  is the angle of the leaving electron beam included by the normal of the surface. The intensity of the electron emission coming from the lowest layer:

$$I_1 = I_{10} \{1 - \exp[-d_1/(\lambda_{11} \cos \vartheta)]\} \prod_{i=2}^n \exp[-d_i/(\lambda_{i1} \cos \vartheta)] \quad (2)$$

while the intensity of emission from the uppermost layer is

$$I_n = I_{n0} \{1 - \exp[-d_n/(\lambda_{nn} \cos \vartheta)]\}. \quad (3)$$

### Square base, chequered pits with walls perpendicular to the surface

The general models are based on two conditions: 1. the roughnesses are smaller than the X ray penetration depth, and 2. they are bigger than the layer thicknesses. These conditions are valid for transition and macropores. The model of chequered pits differs from the planar surface in two aspects: (i) also the side walls emit electrons, and (ii) they shade the emission of the bottom of the pit and that of the other side walls. Shaded surfaces are analogues to areas shaded against the sun. Fig. 1 shows the shadow figures of the bottom and side walls of the pit. Side walls have two kinds of shadow figures, as the bottom plane is not entirely shaded (b) or it is (c).  $\varphi$  is the angle between the projection of the electron beam to the surface and the edges of the pits. If there is only one layer the intensity of the bulk phase, weighted by the area of "one white and one black" square of the chessboard is given by

$$\begin{aligned} I_t = I_{t0} \left\{ \left[ 2 - h \cdot \operatorname{tg} \vartheta (\sin \varphi + \cos \varphi) + \frac{1}{2} h^2 \operatorname{tg}^2 \vartheta \sin 2\varphi \right] \exp\left(-\frac{d}{\lambda \cos \vartheta}\right) + \right. \\ \left. + h \left(1 - \frac{h}{2} \operatorname{tg} \vartheta \sin \varphi\right) \exp\left(-\frac{d}{\lambda \sin \vartheta \cos \varphi}\right) + \right. \\ \left. + h \left(1 - \frac{h}{2} \operatorname{tg} \vartheta \cos \varphi\right) \exp\left(-\frac{d}{\lambda \sin \vartheta \sin \varphi}\right) \right\} \quad (4) \end{aligned}$$

if the horizontal edge of the pits is the unity while  $h$  is their depth. Eq (4) refers to

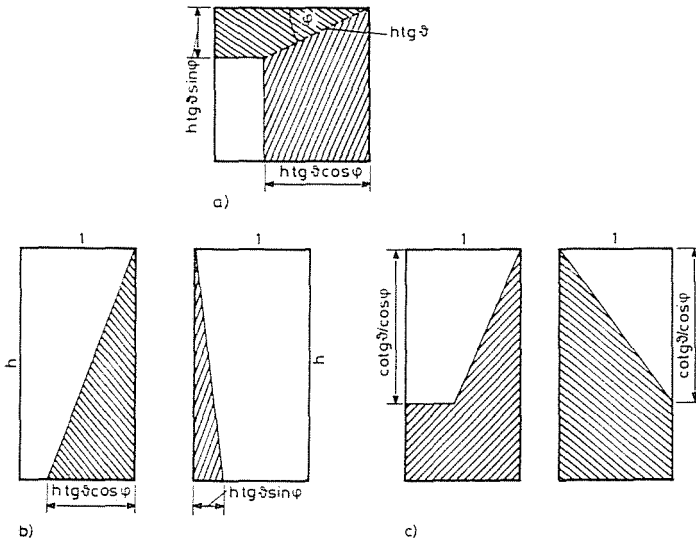


Fig. 1. Image of shadow figures in square base pits. a) Shadow in the bottom of the pit. b) Shadow on side walls when the shadow looks like a. c) Shadow on side walls when the bottom of the pit is entirely shaded

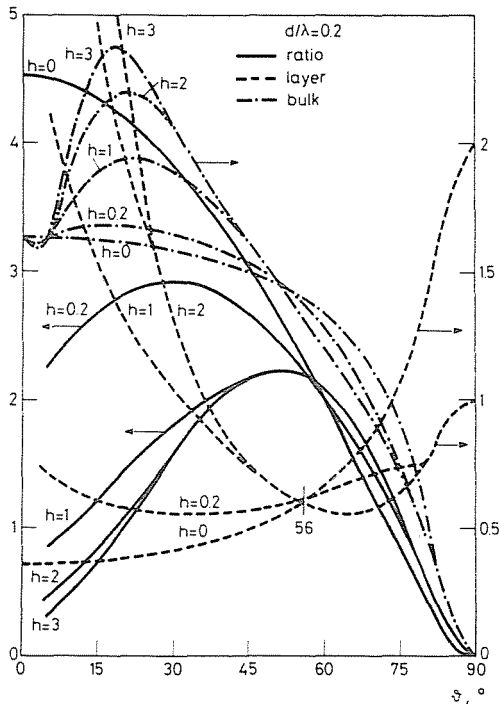


Fig. 2. Peak intensities of bulk and layer electrons in arbitrary units versus  $\vartheta$ . The dependence of the ratio of bulk and layer intensities on  $\vartheta$ .  $d/\lambda = 0.2$ . Chequered model

the case when the bottom of the pit is not entirely shaded. If it is then:

$$I_t = I_{t0} \left[ \exp\left(-\frac{d}{\lambda \cos \vartheta}\right) + \left(1 - \frac{\operatorname{tg} \varphi}{2}\right) \frac{\operatorname{cotg} \vartheta}{\cos \varphi} \exp\left(-\frac{d}{\lambda \sin \vartheta \cos \varphi}\right) + \frac{\operatorname{cotg} \vartheta}{2 \cos \varphi} \exp\left(-\frac{d}{\lambda \sin \vartheta \sin \varphi}\right) \right]. \quad (5)$$

Emission intensities for the bulk phase and surface layer have been calculated (formulae referring to the latter has been modified as far as instead of the exponentials the function  $1 - \exp$  had to be used) varying  $h$  and the ratio  $d/\lambda$ , and averaging the intensities from  $\varphi=0$  to  $\pi/4$ . Figures 2 and 3 show intensity- $\vartheta$  relationship of the electron emission of the bulk and the surface layer in the case of  $d/\lambda=0.2$  and  $d/\lambda=1$ , resp. The ratio of the bulk and the layer intensities are also illustrated on the figures. This is monotonous when the surface is plane, in the present case, however, it forms a maximum curve. The place of the maximum tends to a limit as the pits are deepened. At about  $\vartheta = 55^\circ$  the ratio referring to plane and chequered surfaces is approximately the same, so with a sample turned away from the direction of the spectrometer by  $55^\circ$  the ratio  $d/\lambda$  can be estimated independently of roughnesses. Wagner and Br unner [2] have found this value  $52^\circ$  for one dimensional roughnesses.

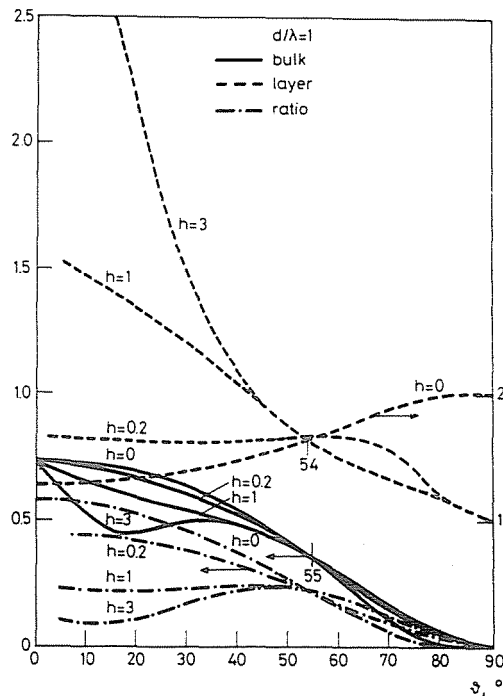


Fig. 3. Peak intensities and their ratio when  $d/\lambda=1$

### Square base pyramid shape pits touching each other by their edges

At low angles  $\vartheta$  the whole pit emits electrons while at higher angles shadow figures of two kinds can occur as can be seen on Fig. 4.  $\beta$  is the slope of the side walls while  $L$  is the distance from the margin of the shadow to the edge of the pit. Calculation of  $L$  can be understood from Fig. 5 showing the stranded shadow from top (a) and from side view (b). From Fig. 5/b:

$$\operatorname{tg} \vartheta = \frac{2 - L \sin \beta}{L \cos \beta \cos \varphi} \text{ hence:}$$

$$L = \frac{2}{\sin \beta + \cos \beta \operatorname{tg} \vartheta \cos \varphi} \quad (6)$$

The intensity of the bulk phase if the whole pit is unshaded:

$$I_t = I_{t0} \frac{1}{\sin \beta} \sum_{i=1}^4 \exp(-d/A_i) \quad \text{where} \quad (7)$$

$$A_1 = \lambda (\sin \beta \cos \vartheta + \cos \beta \sin \vartheta \cos \varphi),$$

$$A_2 = \lambda [\sin \beta \cos \vartheta + \cos \beta \sin \vartheta \cos (\varphi + 270^\circ)],$$

$$A_3 = \lambda [\sin \beta \cos \vartheta + \cos \beta \sin \vartheta \cos (\varphi + 90^\circ)] \quad \text{and}$$

$$A_4 = \lambda [\sin \beta \cos \vartheta + \cos \beta \sin \vartheta \cos (\varphi + 180^\circ)].$$

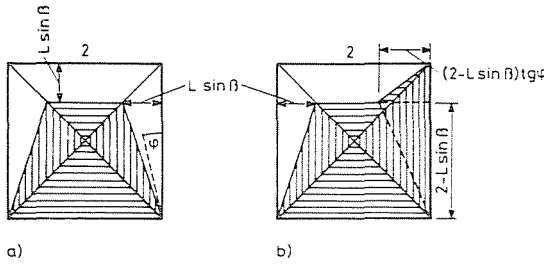


Fig. 4. Shadow figures in pyramid shape pits. Top view. a) Only one side wall is entirely shaded. b) Two side walls are entirely shaded

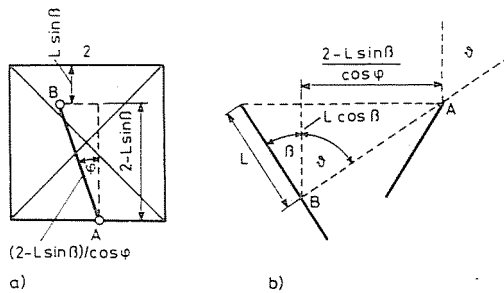


Fig. 5. Parameters of the shadow. a) Top view. b) Side view

The  $A$ -s correspond to the four side walls. If only one side wall is entirely shaded:

$$I_t = I_{t0} \left[ (2 - L \sin \beta) L \exp(-d/A_1) + L \sum_{i=2}^3 \exp(-d/A_i) \right]. \quad (8)$$

If two sides are entirely shaded:

$$I_t = I_{t0} \left\{ \left[ 2 - \frac{L \sin \beta}{2} (1 - \operatorname{tg} \varphi) - \operatorname{tg} \varphi \right] L \exp(-d/A_1) + L \exp(-d/A_2) \right\}. \quad (9)$$

When calculating layer intensities instead of exponentials again the corresponding  $1 - \exp$  functions have to be applied. In the calculations  $\beta$  and the ratio  $d/\lambda$  have been varied and the calculated intensities have been averaged from  $\varphi = 0$  to  $\pi/4$ . The dependence of the intensities on  $\vartheta$  will be discussed in comparison to the following model.

### Square base pyramids touching each other by their bottom edge

At small angles  $\vartheta$  all four side walls are unshaded, at somewhat bigger angles we have only three unshaded walls (Fig. 6/a) and increasing  $\vartheta$  further, eventually we have only two (Fig. 6/b). In the latter case because of the enormous variety of shadow figures the calculation of the intensities is very complicated. This statement can be characterized by the fact that while the program varying  $\vartheta$ ,  $\varphi$ ,  $\beta$  and  $d/\lambda$  consisted for pyramid shape pits of 42 steps, for pyramids it involved 231 steps. Figs 7 and 8 show the emission intensities of the pits and the pyramids in comparison at two different values of  $d/\lambda$ . The curves are strikingly similar suggesting that the calculation of the whole and very complicated pyramid program is not necessary. A characteristic feature of layer intensities and consequently that of intensity ratios is a breaking point at  $\beta = \vartheta$ .

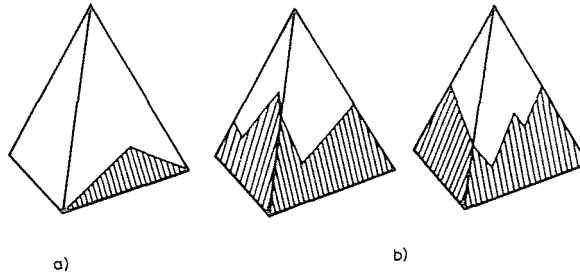


Fig. 6. Shadow figures on pyramids, a) Only one side wall is shaded. b) Two types of shadow when two side walls are entirely shaded

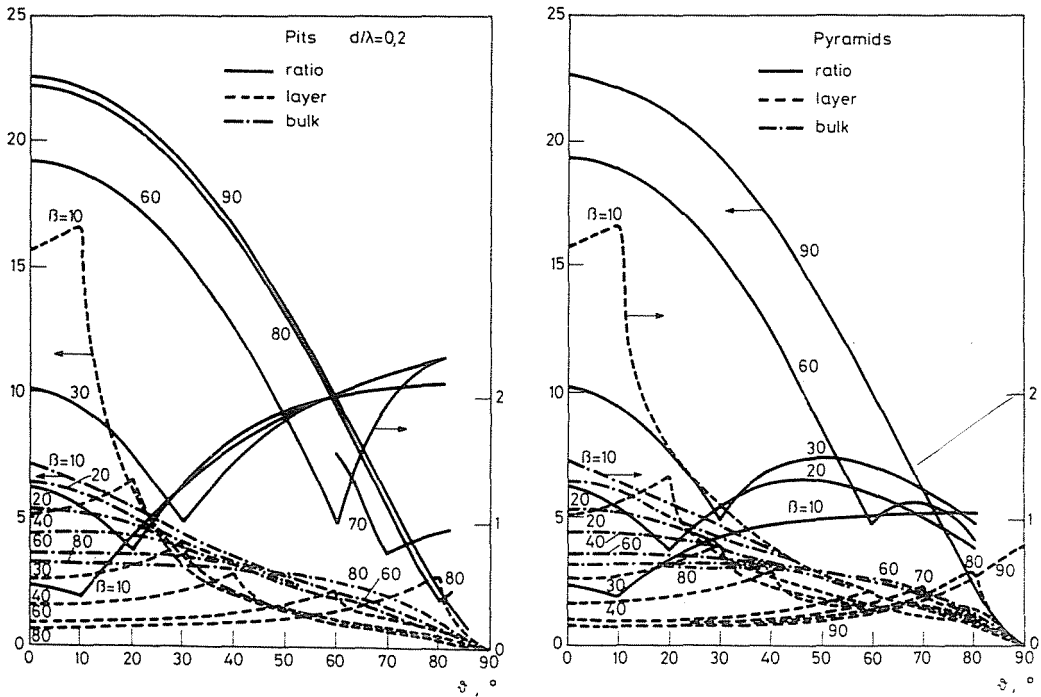


Fig. 7. Peak intensities of bulk and layer electrons a) coming from pyramid shape pits or b) from the surface of pyramids in arbitrary units versus  $\vartheta$ . The ratio of bulk and layer intensities also illustrated.  $d/\lambda=0.2$

At somewhat lower angle  $\vartheta$  than the critical one the electron beam steps out almost tangentially, thus, the layer emission is dominant, at somewhat higher angles, however, the side wall hitherto radiant, will be enveloped in shadow and does not emit more electrons.

If crystallite faces mounted on a plane crystal face have some dominant angle then—in order to avoid diffraction phenomena—covering the whole surface by a non-crystalline layer, this dominant angle will be betrayed by the angle resolved intensities of the layer emission. (During XPS measurements every sample will be covered by a layer of carbon compounds. The carbon emission itself can indicate the angle between the new crystal faces and the plane of the monocrystal.)

At  $\vartheta=55^\circ$  the intensity ratios calculated from peaks measured for emission from planar surfaces, pits and pyramids of different steepness have a higher deviation than for the chequered model but their average is still characteristic of the ratio  $d/\lambda$ . Fig. 9 illustrates the bulk-layer intensity ratios as a function of  $d/\lambda$ , labelling also the deviations of different models.

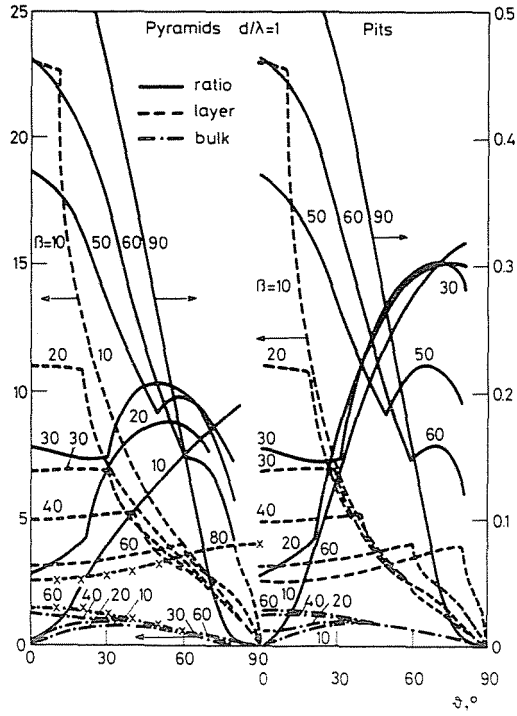


Fig. 8. Bulk and layer intensities and their ratio. Pits and pyramids.  $d/\lambda=1$

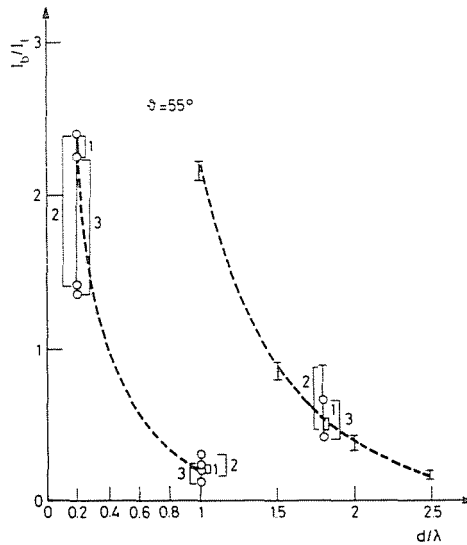


Fig. 9. Bulk-layer intensity ratio versus  $d/\lambda$ . Deviations have their origin from different models (planar surface, chequered model, pyramid shape pits and pyramids).  $\vartheta=55^\circ$ . 1=chequered, 2=pits, 3=pyramids

### Spheres in closest packing with a tangent-plane surface

This model stands very near the flattened surfaces of powder samples. The intensity of the bulk emission integrated to a hemisphere:

$$I_t = I_{t0} \int_0^{\pi/2} \int_0^{2\pi} \sin \vartheta \exp[-d/(\lambda \cos \vartheta)] d\vartheta d\varphi. \quad (10)$$

The integral cannot be analytically solved, therefore the hemisphere had to be divided into segments of  $10^\circ$  width whose area is  $2 \sin 5^\circ \sin \vartheta$ , in multiples of  $2\pi$  where  $\vartheta$  is the average angle of the segment. For the surface in closest packing the (111) plane of the face centred cubic lattice was chosen. The characteristic feature of this section is that among the six leaks bordering a surface sphere there is a sphere of the second layer under three ones and there is a sphere of the third layer under the other three ones. Looking from above these spheres are also "visible", thus, one has to consider their emission in addition. In this sense for example the area of the calotte from  $0$  to  $10^\circ$  has to be multiplied by 2.832 because of the contribution of the lower layers. Only the segment between  $30$  and  $40^\circ$  has not to be completed by the radiant areas of the lower layers.

If the electron beam is not perpendicular to the tangent plane, the neighbouring spheres more or less shade each other. Fig. 10 regards the spheres from the direction of the electron beam. On the figure the spheres are in two singular positions averaged in the calculations. From such a view, the points from which the electrons step out in identical angle form concentric circles with a radius of  $\sin \delta$ . Segment areas belonging to these concentric circles are equal to  $2 \sin 5^\circ \sin \delta$  if, according to our choice, the circles are spaced to  $10^\circ$ . On Fig. 11 the projection of the distance between both spheres to the plane

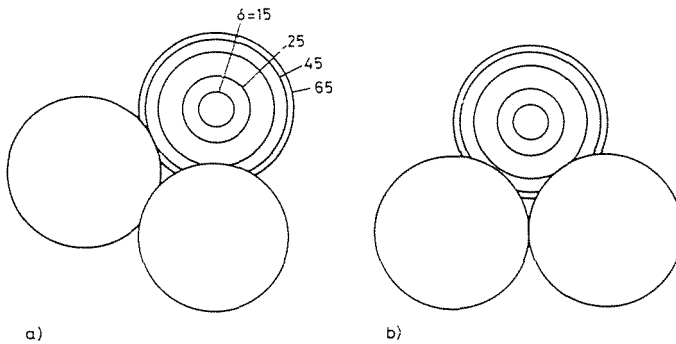


Fig. 10. Mutual shading of spheres in closest packing in two positions.  $\vartheta = 35^\circ$

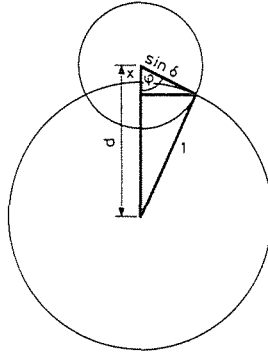


Fig. 11. Shading of parallels of latitude by the neighbouring sphere

perpendicular to the electron beam is denoted by  $d$ . The common right angle side of the two rectangular triangles is:  $\sin^2 \delta - x^2 = 1 - (d - x)^2$ . Hence:

$$x = \frac{1}{2} \left( d - \frac{\cos^2 \delta}{d} \right).$$

The central angle of the covered circular arc equals to  $2 \cos^{-1} \varphi$  where  $\cos \varphi = \frac{1}{2 \sin \delta} \left( d - \frac{\cos^2 \delta}{d} \right)$ . It has been calculated at different  $\vartheta$ -s what proportion of the segments belonging to different  $\delta$ -s is shaded by neighbouring spheres. The bulk and layer intensities and their ratio can be seen on Fig. 12. The points denoted off the curves at  $\vartheta = 35^\circ$  may be interpreted as the ideal behaviour of the model. In the case of closest packing, namely from a direction of  $35^\circ$  from the normal one can "see into" down till about forty layers so that many spheres can emit electrons from considerable depths stepping out in very small angles thus coming mainly from the surface layer enhancing the layer intensity singularly.

### Ion etching on sphere shaped surfaces

Ion etching is a direct method for studying surface layer structures. If a plane surface is etched by sweeping mode one can obtain an etched plane approximately parallel to the surface. In this case the layer thicknesses can be determined from the intensity variation if the etching depth is known. In the case of rough surfaces, however, the result is not unanimous. The effect of ion etching on spheres in closest packing has been studied in order to get some information also about ion etching of powdered samples. The ion gun shoots the ions to the sample surface at an angle of  $45^\circ$  because the etching is the most effective from this direction. Two functions, in agreement with the experience, have been applied for the effectiveness of etching. For angles less than  $45^\circ$ :  $I = m(0.8 + 0.2 \sin^2 2\gamma)$  where  $m$  stands for the etching depth and  $\gamma$  is the etching

angle. For angles bigger than  $45^\circ$  :  $I = m \cos (2\gamma - \pi/2)$ . If the incident ion beam closes an angle of  $45^\circ$  with the macroscopic surface, then  $\gamma = \pi/4 + \vartheta \cos \beta$  where  $\beta$  is the azimuth of the etched point measured from the direction of the ion beam. In averaging the intensities of the emission from the etched points over all  $\vartheta$ -s and  $\beta$ -s, being the angle of ion incidence really  $45^\circ$ , also the shading of the other spheres for the etching has been taken into account. Fig. 13 shows

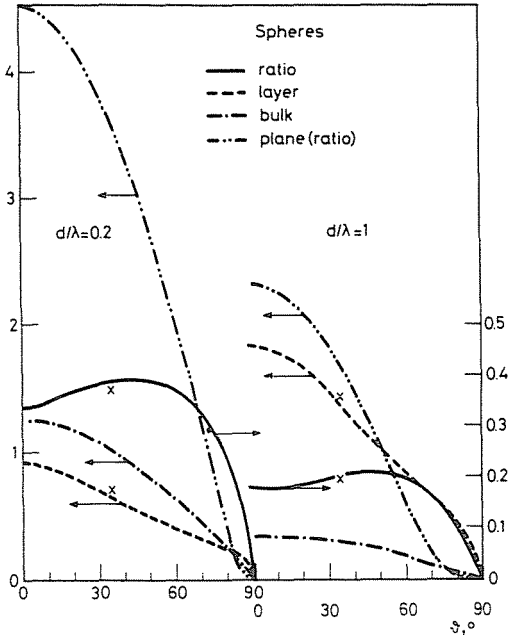


Fig. 12. Bulk and layer intensities and their ratio versus  $\vartheta$ . Electrons coming from spheres in closest packing.  $d/\lambda$  are 0.2 and 1, resp

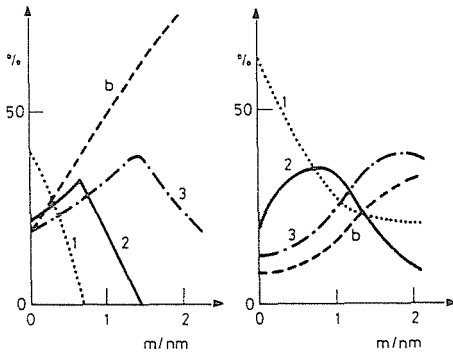


Fig. 13. Intensity variations as a result of ion etching of planar surfaces and of spheres in closest packing. Curves labelled by 1, 2 and 3 belong to layers while the letter b denotes bulk phase

an example for the result of ion etching on planar surface using sweeping mode, and on a surface consisting of spheres. On the ordinate axis intensity percentages are given while the abscissa informs us about the etching depths. The bulk phase is covered by three layers. The thickness of the lowest one is 1.4 nm while both upper layers are 0.7 nm thick.

## Applications

### *a) Forming of a $\text{SiO}_2$ layer on $\gamma\text{-Al}_2\text{O}_3$*

When  $\gamma\text{-Al}_2\text{O}_3$  reacts with  $\text{SiCl}_4$  a solid  $\text{SiO}_2$  layer is built on the bulk material. A specific surface of  $160 \text{ m}^2/\text{g}$  could be reproduced by cubic particles with an average edge length of 10 nm (Fig. 14). The clods shown on the figure can occur in every orientation. Kuipers [3] has modelled the different orientations by hemispheres, in that model, however, the shading was not taken into account though it is always present on porous surfaces. Silicone content has been determined by two independent methods, atomic absorption spectroscopy and XPS. [4] The former gives the total composition while the latter informs about the surface phase. The molar fraction of Si in samples with different Si contents, determined by atomic absorption proved to be constantly 0.66 times as much as when measured by XPS.

Four models have been constructed (Fig. 15). A uniform 0.3 nm carbon compound thickness covering the surface has been supposed. On the abscissas the number of molecular layers containing silicon are displayed. It can be seen that a pure  $\text{SiO}_2$  layer has been supposed only in the case c); in the three other

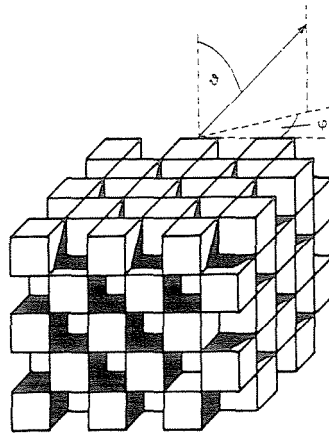


Fig. 14. A model for  $\gamma\text{-Al}_2\text{O}_3$  with a specific surface of  $160 \text{ m}^2/\text{g}$

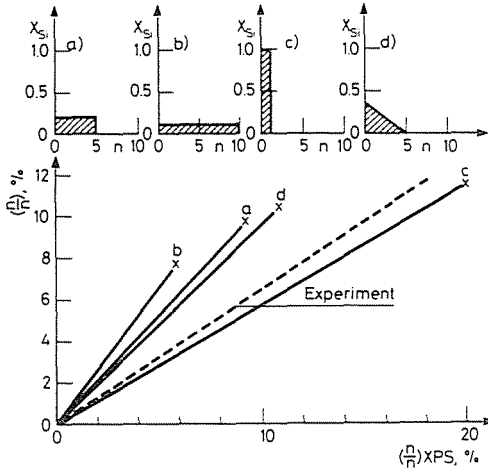


Fig. 15. Below: Molar percentage of Si determined by atomic absorption spectrum versus molar percentage measured by XPS. Dotted line refers to experiment, full lines are calculated according to models labelled by letters. Above: Four models for calculation: a) Molar fraction of Si: 0.2, layer thickness of the composite phase amounts to five molecules. b) Molar fraction 0.1, thickness of ten molecules. c) Pure  $SiO_2$ , thickness is one molecule. d) Changing molar fraction from 0.4 to 0. Whole thickness amounts to five molecules

cases composite phases have been assumed. In the intensity formulae the electron flux proportional to  $I_0$  can be given in the product form [5]:

$$I_0 \sim N_A k_1 c \rho \alpha \lambda \tag{11}$$

where  $N_A$  is the Avogadro constant,  $k_1$  is the rate coefficient of photoemission,  $c$  is the concentration of the emitting material,  $\rho$  is the density of X-ray photons,  $\alpha$  is the solid angle and  $\lambda$  is the escape depth.  $k_1 \rho = \sigma j^R$  where  $\sigma$  is the cross section of photoemission while  $j^R$  stands for the X-ray flux. On the other hand  $\lambda = u/(k_2 c) = \sqrt{2T/m}/(k_2 c)$  where  $u$  is the velocity of the electron,  $T$  is its kinetic energy,  $m$  is the electron mass,  $k_2$  denotes the rate coefficient of the unelastic collisions of the electrons with atoms, while  $c$  is concentration of the material able to collide with electrons [5]. The experimental cross sections published in the literature:  $\sigma' = \sigma \sqrt{2/m}/(k_2 c)$  where  $c$  is the concentration of the pure material to which the cross section refers. If, however, the electron comes from a composite phase in which the escape depth differs from that in the emitting pure material, the intensities have to be corrected by  $V_m/V_{m0}$  ( $V_m$  is the molar volume of the composite phase while  $V_{m0}$  belongs to the pure phase).

In the fourth model of Fig. 15 a varying concentration is assumed. If  $x^s$  is the molar fraction at the upper limit of the layer while  $x$  is the molar fraction

inside and  $b$  is the molar fraction gradient, then instead of

$$x \left[ 1 - \exp \left( - \frac{d}{\lambda \cos \vartheta} \right) \right] = \frac{x}{\lambda \cos \vartheta} \int_0^d \exp \left( - \frac{z}{\lambda \cos \vartheta} \right) dz,$$

the expression

$$\frac{1}{\lambda \cos \vartheta} \int_0^d (x^s + bz) \exp \left( - \frac{z}{\lambda \cos \vartheta} \right) dz$$

has to be integrated.

On the basis of Fig. 14 the intensities of Figs 2 and 3 have been averaged to the whole region taking into consideration the corresponding  $d/\lambda$  ratios. The straight lines of Fig. 15 have been obtained by this procedure. One can state that the model c) stands nearest the molar fraction ratio 0.66 obtained from atomic absorption spectroscopy related to XPS. One can establish from this that there is no composite phase:  $\text{SiO}_2$  covers  $\text{Al}_2\text{O}_3$  in the form of a *unimolecular layer*.

#### b) Coating of $\text{TiO}_2$ by $\text{SiO}_2$ and $\text{Al}_2\text{O}_3$

Having determined the specific surface of  $\text{TiO}_2$  it was established that the average radius of the supposingly nearly sphere shaped  $\text{TiO}_2$  particles amounts to 92.5 nm. The molar fractions of Si and Al have been calculated from atomic absorption measurements. From these data the layer thicknesses of  $\text{SiO}_2$  and  $\text{Al}_2\text{O}_3$  could be determined for a multiple spherical shell model. With these thicknesses and a layer thickness of carbon compounds estimated to 0.3 nm and using the smooth spherical model the following molar ratios have been obtained: C 1.40, Si 0.54, Ti 0.37, related to aluminium. On the other hand the ratios measured by XPS and converted to molar fractions are as follows: C 1.75, Si 0.29 and Ti 0.49. As the calculated Si amount is almost twice as much as the measured one even supposing that the  $\text{SiO}_2$  layer is *under* the  $\text{Al}_2\text{O}_3$  layer, the smooth spherical shell model had to be rejected. One gets nearer to the solution supposing a porous  $\text{Al}_2\text{O}_3$  layer above  $\text{SiO}_2$  when the inside walls of the pores also get covered by the carbon compound which diminishes to a higher extent the intensity of Si than that of the Al electrons.

The spherical and chequered models were combined: the sphere of  $\text{TiO}_2$  is enveloped by a 1.303 nm thick  $\text{SiO}_2$  layer. Above this layer the  $\text{Al}_2\text{O}_3$  cubes are settled in a chequered formation i.e. touching each other by their vertical edges. The edge lengths are 1.34 nm. The layer thickness of carbon compounds is 0.2 nm "fattening" however the cubes so that a spherical surface is formed with square shaped pores. The edge length of a pore square is 0.94 nm, their distance perpendicularly to their edges is 1.74 nm. The calculated molar ratios

related to Al are: C 1.41, Si 0.40. Supposing the inside carbon thickness to be 0.3 nm the ratios: C 1.80, Si 0.40. This latter approaches the measured datum of 0.29 better than the value of 0.54 coming from the smooth spherical model but the difference is still considerable. Taking, however, into account—as demonstrated in different experiments—that the  $\text{TiO}_2$  can diffuse into the  $\text{SiO}_2$  layer and if instead of a compact  $\text{SiO}_2$  layer, one calculates with two composite layers (Si molar fractions would be 0.7 and 0.3) an intensity ratio Si/Al of 0.30 can be obtained. Using this model the ratio Ti/Al proved to be 0.35. If, however, only 8% of  $\text{TiO}_2$  would be uncovered the experimental ratio 0.49 becomes right. In this latter case the ratio of carbon is 1.75.

### References

1. FADLEY C. S.—BAIRD B. J.—SIEKHAUS W.—NOVAKOV T.—BERGSTRÖM S. A. L.: *J. Elect. Spect. Rel. Phen.* 4, 93 (1974).
2. WAGNER N.—BRÜNNER O.: *Exp. Tech. Phys.* 29, 6, 571 (1981).
3. KUIPERS P. C. E.: *Solid State Ionics* 16, 15 (1985).
4. VARSÁNYI GY.—BERTÓTI I.—MINK GY.—RÉTI F.—RÉVÉSZ M.: *MTA Kém. Közl.* (in press)
5. VARSÁNYI GY.—VESZPRÉMI T.—BERTÓTI I.: *Fotoelektron-spektroszkópia. BME Mérn. Tovk. Int. Budapest* (1985).

Prof. Dr. György VARSÁNYI }  
Katalin RÉE } H-1521 Budapest

György MINK } Magyar Tudományos Akadémia  
Miklós MOHAI } H-1051 Budapest